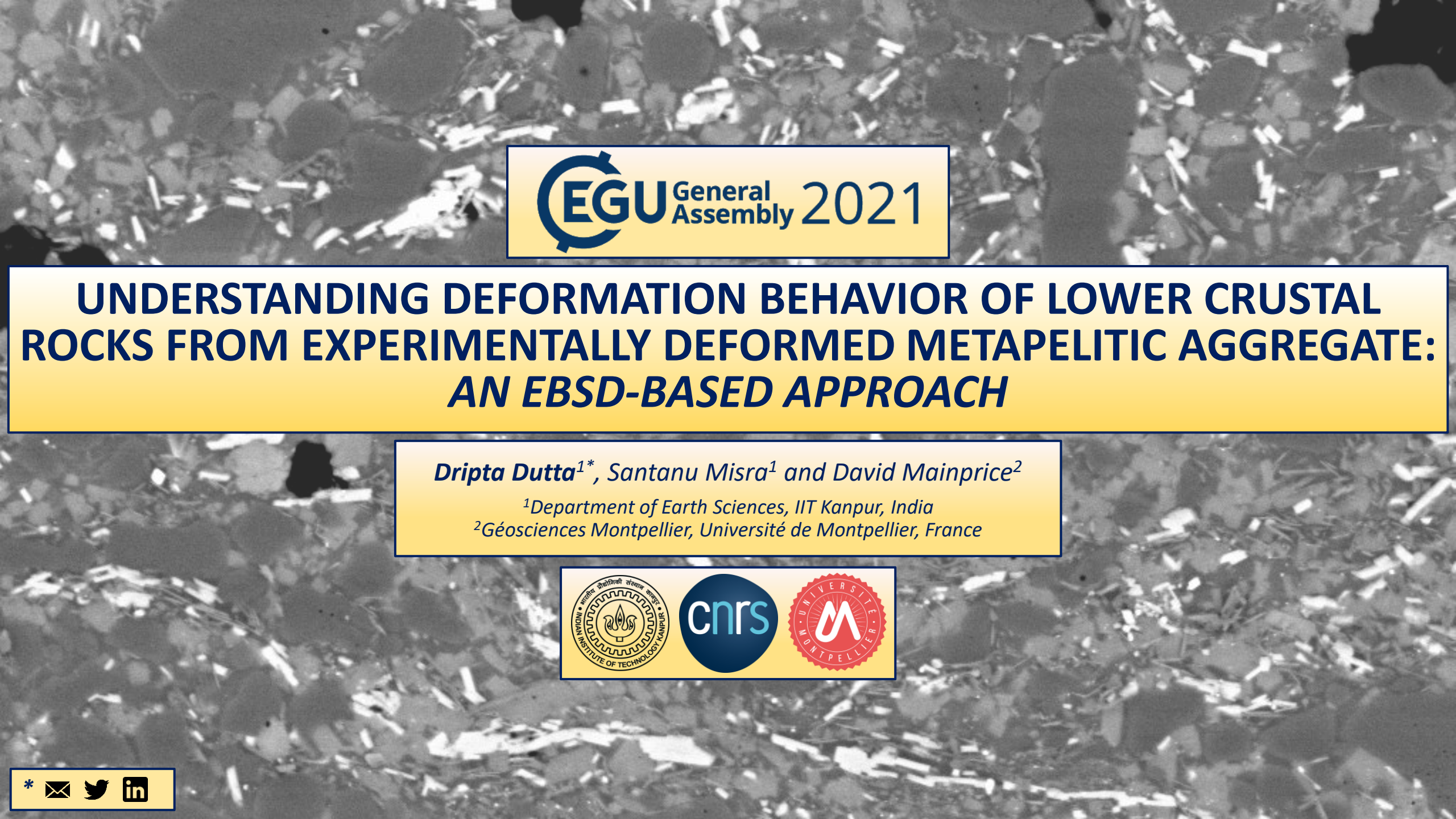

EGU General Assembly 2021

UNDERSTANDING DEFORMATION BEHAVIOR OF LOWER CRUSTAL ROCKS FROM EXPERIMENTALLY DEFORMED METAPELITIC AGGREGATE: *AN EBSD-BASED APPROACH*

***Dripta Dutta*[1*], *Santanu Misra*[1] *and David Mainprice*[2]**

[1]*Department of Earth Sciences, IIT Kanpur, India*
[2]*Géosciences Montpellier, Université de Montpellier, France*

* ✉ 🐦 in

What is known so far?

- Generation of partial melts at lower crustal levels is well known, and its effects on the strength of the host rock has also been evaluated through laboratory experiments (Misra et al. 2014, JGR SE; van der Molen & Paterson 1979, CMP).

- It has also been reported that the dominating deformation mechanism switches from dislocation creep at low melt fractions (1-4%) to grain boundary sliding once the melt fraction exceeds 7% (Hasalová et al. 2008, JMG).

- Crystallographic preferred orientation (CPO) of deformed minerals reflects the intra-crystalline plasticity accommodated by dislocation creep mechanism. Diffusion creep with or without grain boundary sliding can also produce a CPO, however, its strength would be much weaker.

- Mere presence of a strong CPO may not indicate deformation by dislocation creep since deformation induced preferred alignment of elongated grains both syn- or post growth may also generate the same.

What are we interested in and why?

- During deformation of migmatites, the mineral assemblages including the melt derived phases may deform by dislocation creep (Miranda & Klepeis, 2016). However, not much has been reported on the deformation behavior of the phases crystallizing '***in-situ***' from the melt, under dynamic conditions. This is mostly because, the processes happen at depth and the initial deformation features are overprinted or destroyed by further deformation.

- We focus on the deformation behavior of the '***in-situ***' crystallized phases derived from the partial melt in a metapelitic assemblage – analog to the lower crust – with increasing shear strain using EBSD-based microtextural analysis.

- **How could the shear induced directional growth of phases – if any – influence intragranular deformation?**

- **How does rotation of the '*in-situ*' crystallized phases impact their corresponding CPOs?**

Deformation experiment

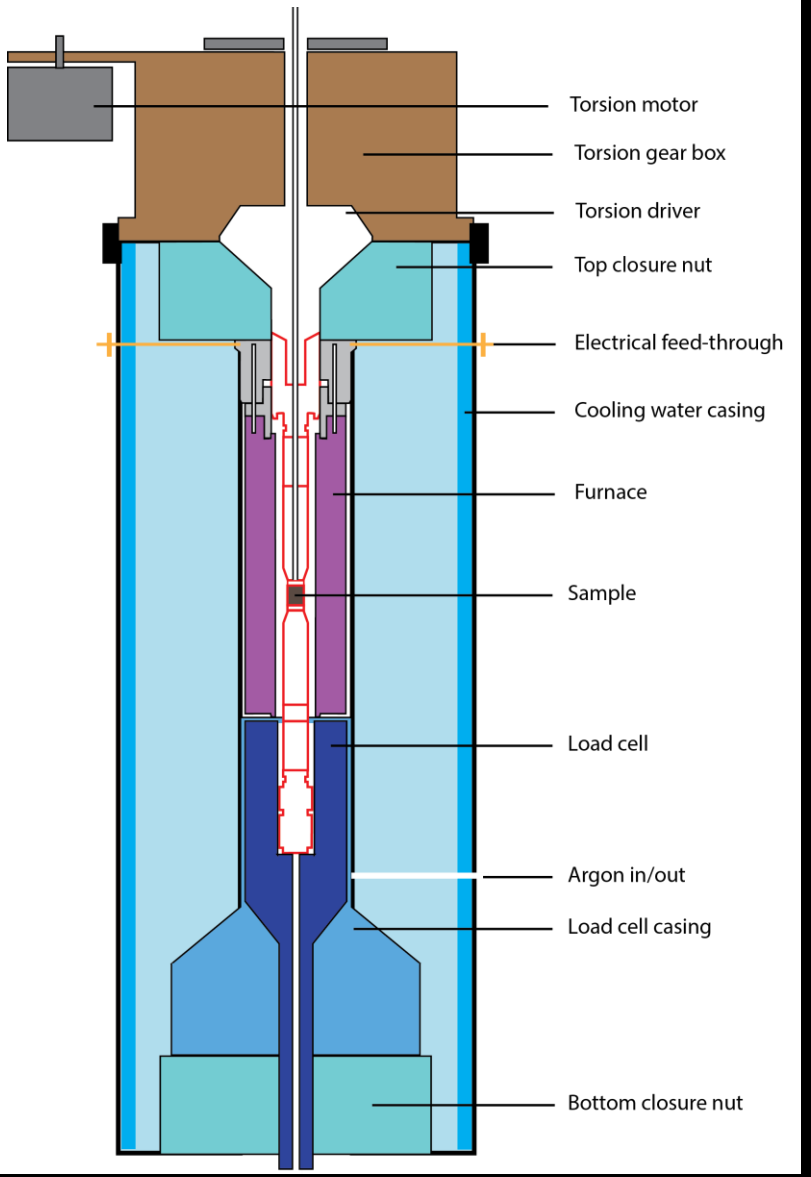

Fig. 1. *Schematic illustration of the Paterson-type deformation apparatus.*

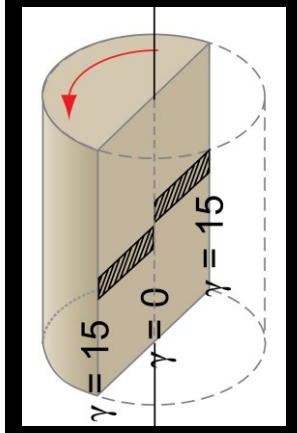

Fig. 2. *Schematic illustration of a deformed cylindrical sample (10 mm diameter) under torsion, cut along the longitudinal axial section. The black striped zones on the longitudinal axial face show the locations along which EBSD data were obtained. The magnitude of shear strain increases from the center to the edge of the cylinder.*

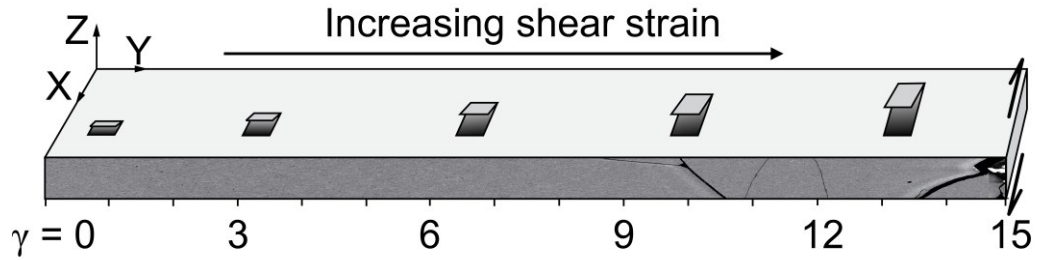

Fig. 3. *Block diagram representing one of the stripped zones showing the standard shear kinematic reference axes (XYZ), shear sense and the SEM image of the observed longitudinal axial section (YZ) of the sample.*

- **Starting material** = homogeneous mixture of Quartz + Muscovite powder
- Uniaxially cold pressed at 200 MPa and then isostatically hot pressed for 24 hours at 160 MPa and 580 °C.
- The deformation was conducted at a constant shear strain rate of 3 x 10-4 s^{-1}, 300 MPa confining pressure, & 750 °C.

Electron backscatter diffraction

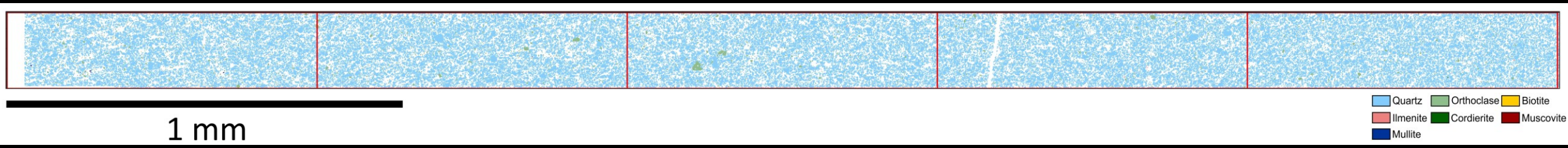

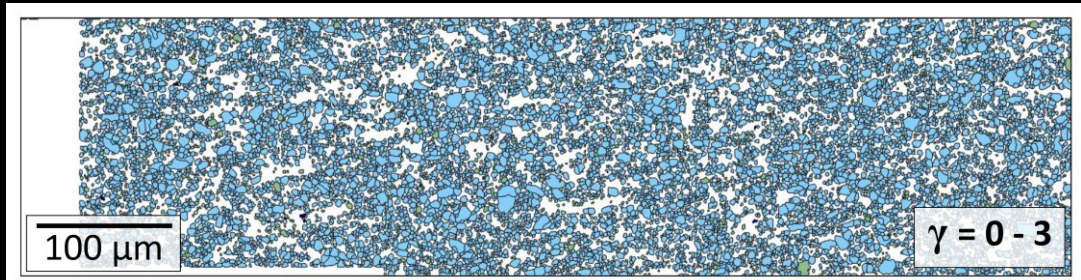

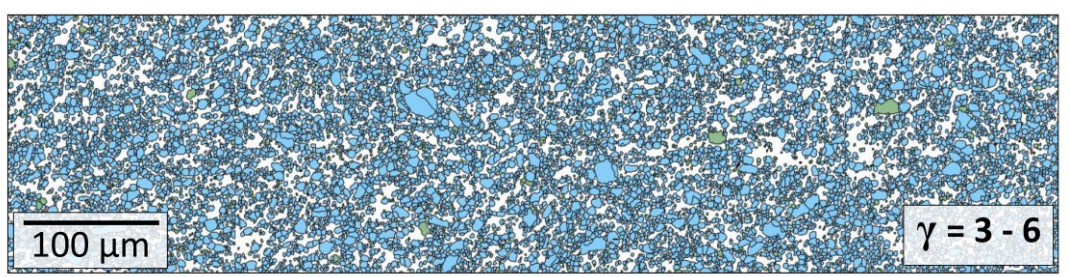

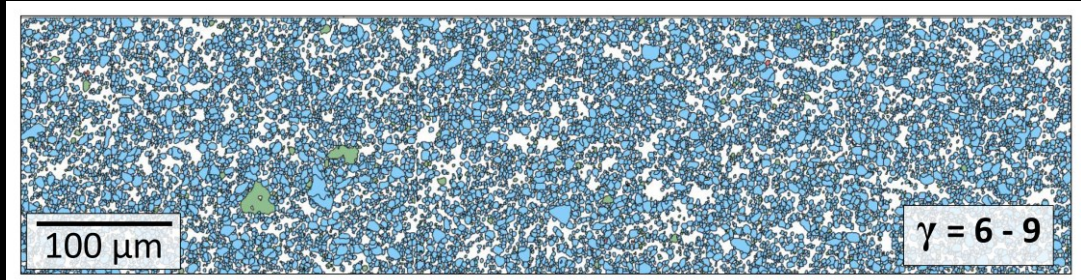

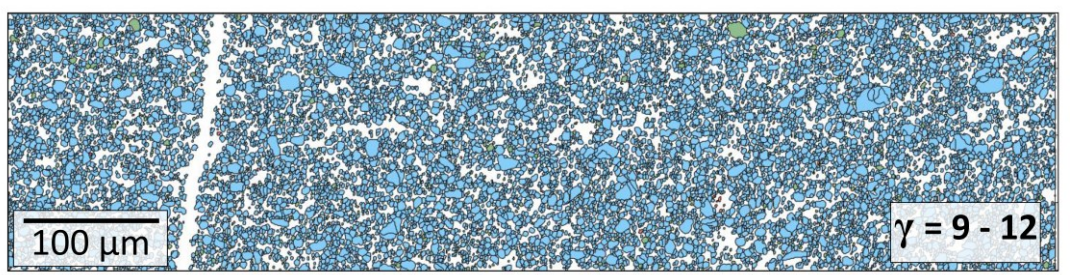

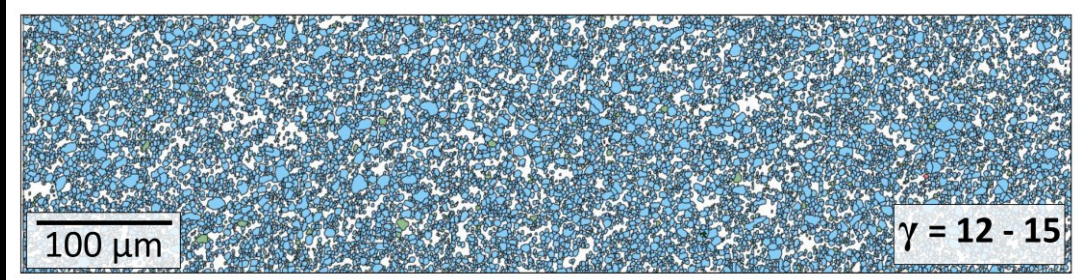

Fig. 4. *Phase map of one of the strips from Fig. 2. The red rectangles demarcate the subregions of varying shear strains. The phase maps corresponding to each of these five subregions are also shown (Dutta et al., under review, GRL).*

[001] Pole figures v/s Shear strain

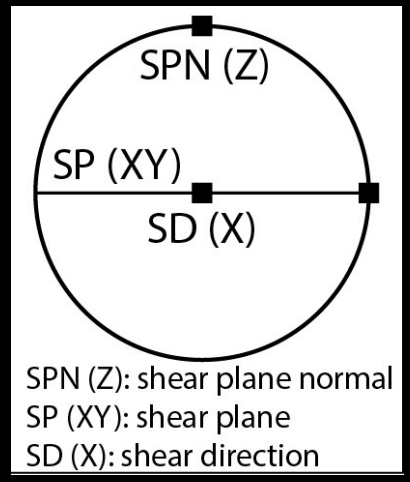

Fig. 5. *Schematic illustration showing the pole figure reference frame*

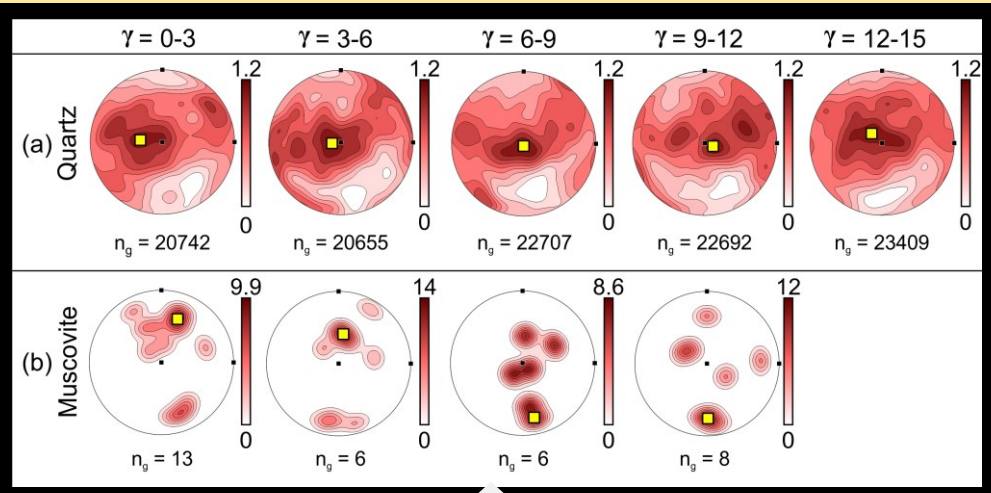

Initial phases

'In-situ' crystallized phases

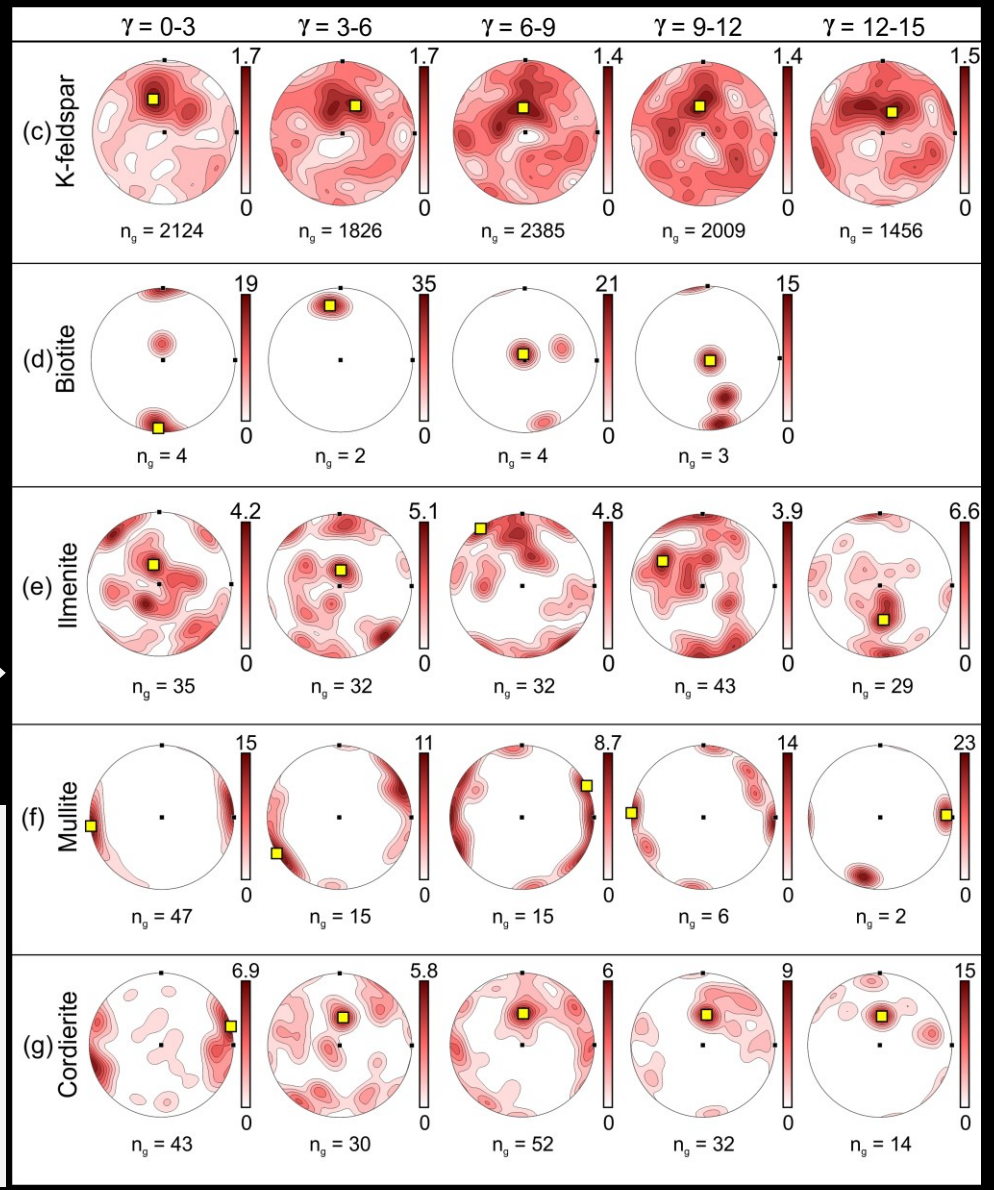

Fig. 6. *Variations in [001] 'one-point-per-grain' pole figures indices with increasing shear strain. The yellow squares inside each pole figure represent the point corresponding to the maximum intensity. All the pole figures are equal-area, lower hemispheric stereographic projections contoured to multiples of uniform density. No grains were detected for muscovite and biotite in the region corresponding to γ = 12-15. n_g = number of grains (Dutta et al., under review, GRL).*

CPO strength indices v/s Shear strain

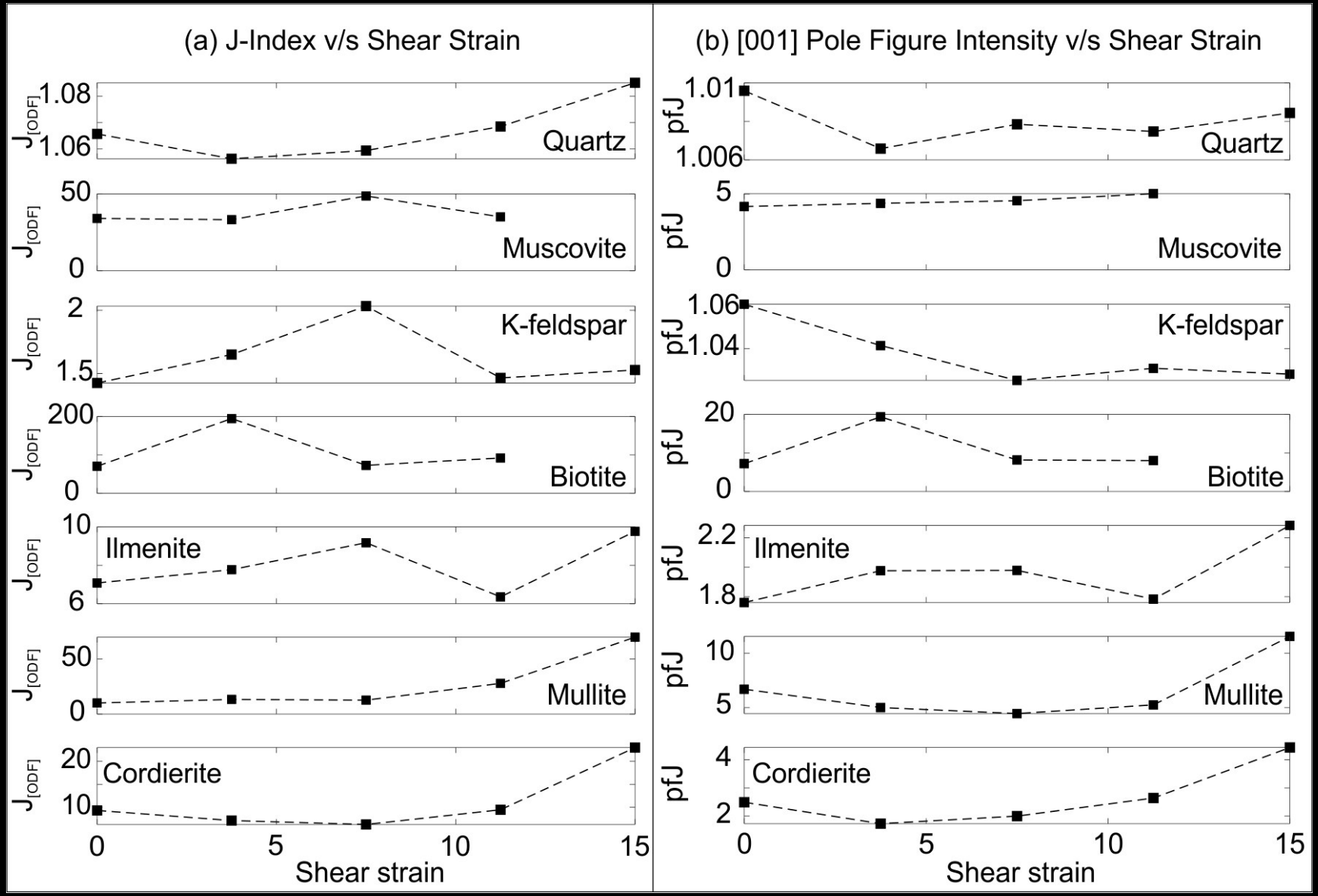

Fig. 7. *Variations in the CPO strength indices with increasing shear strain. No grains were detected for muscovite and biotite in the region corresponding to γ = 12-15. $J_{[ODF]}$ = J-index; pfJ = pole figure intensity (Dutta et al., under review, GRL).*

High angle (> 10°) neighbor-pair misorientation v/s Shear strain

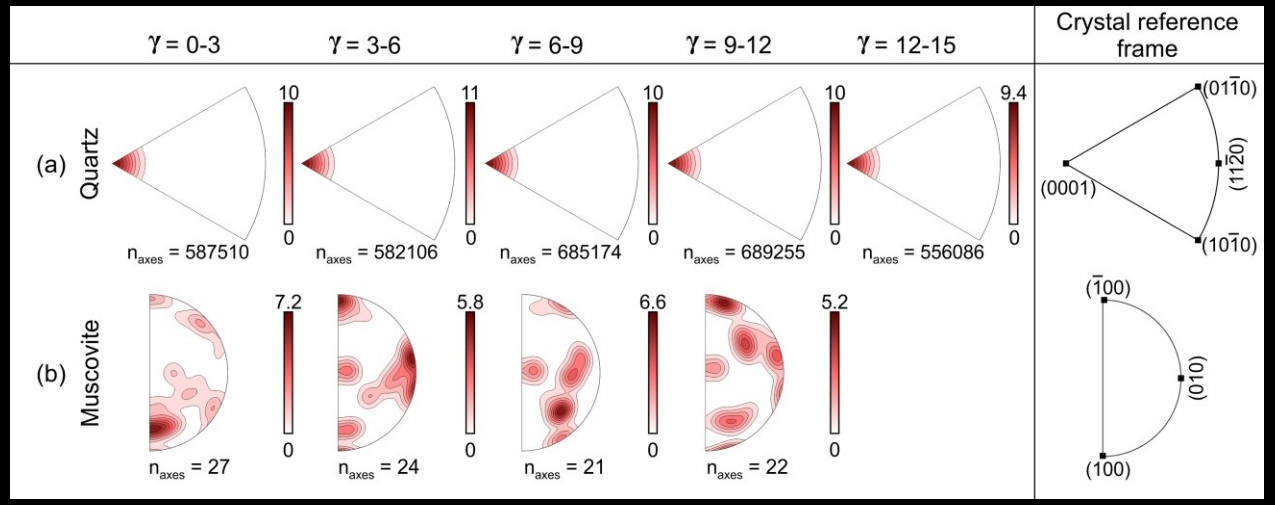

Initial phases

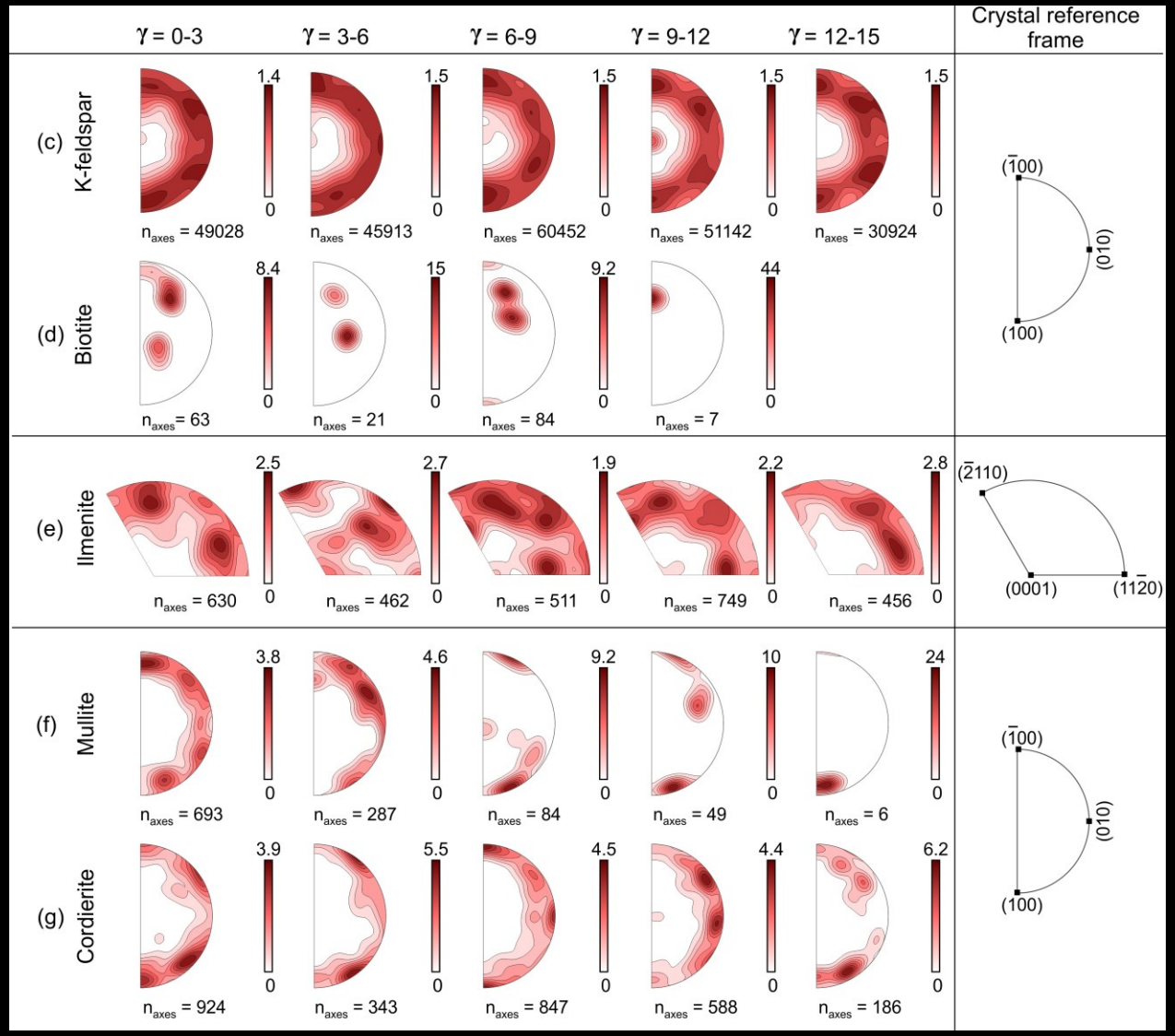

'In-situ' crystallized phases

Fig. 8. *Inverse pole figures (IPF) of high angle (> 10°) misorientation axes plotted on respective crystal coordinate systems as shown on the extreme right column. Each IPF is contoured to multiples of uniform density. n_{axes} = number of high angle misorientation axes (Dutta et al., under review, GRL).*

Shape preferred orientation v/s Shear strain

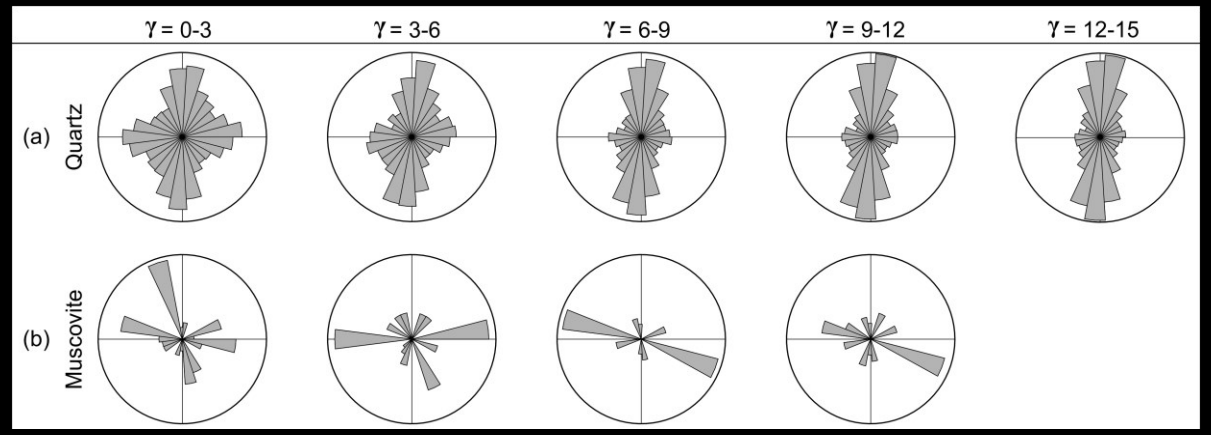

Initial phases

'In-situ' crystallized phases

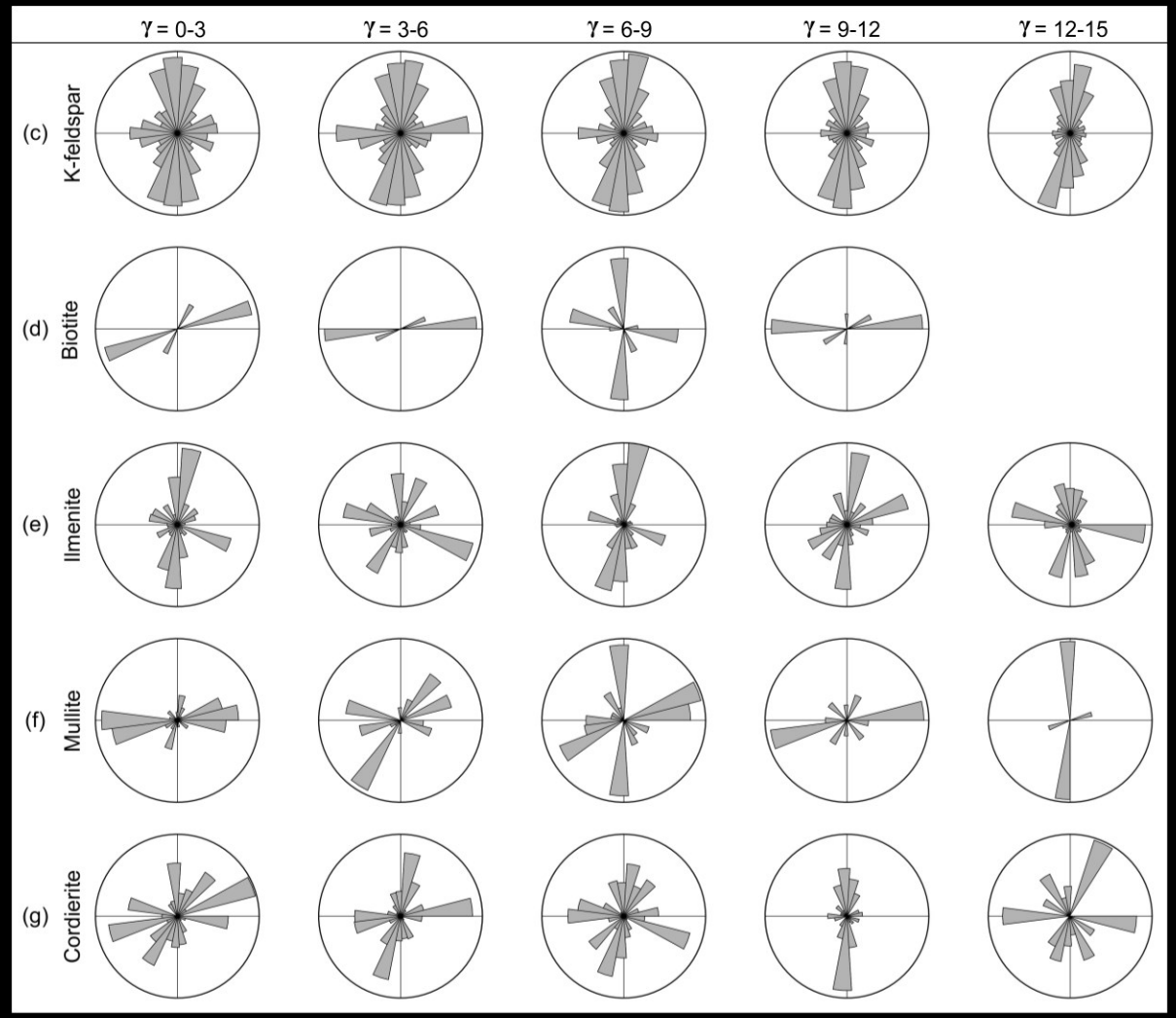

Fig. 9. *Rose diagrams depicting the variation in the shape preferred orientations (long axis) of the grains of each phase with increasing shear strain. The horizontal and vertical lines in the rose plots represent the traces of the XY and XZ planes, respectively (Dutta et al., under review, GRL).*

What did we learn?

- Melt-assisted diffusion creep and grain boundary sliding were the dominant mechanisms through which the grains – both initial and melt-crystallized – deformed.

- Amongst the '*in-situ*' crystallized phases those with equidimensional grains viz. K-feldspar, cordierite and ilmenite underwent syn-torsional 'rigid body rotation', which was enhanced by the presence of surrounding melt and eventually faded as the crystal:melt ratio rose at $\gamma > 7$.

- Strong CPOs exhibited by muscovite, biotite and mullite grains are not a consequence of intense intra-crystalline deformation/dislocation creep mechanism, but rather have been derived from the SPO that resulted due to the preferential growth of the long axes of these grains within the shear plane.

Understanding deformation behavior of lower crustal rocks from experimentally deformed metapelitic aggregate: an EBSD-based approach (EGU21-14101)

Dripta Dutta[1], Santanu Misra[1], and David Mainprice[2]

driptad@iitk.ac.in

[1]Department of Earth Sciences, IIT Kanpur (India), [2]Géosciences Montpellier, Université de Montpellier (France)

1. Background

- Generation of partial melts at lower crustal levels is well known.
- Dominating deformation mechanism switches from dislocation creep at low melt fractions (1-4%) to grain boundary sliding with > 7% melt.
- Crystallographic preferred orientation (CPO) of deformed minerals reflects the intra-crystalline plasticity accommodated by dislocation creep mechanism. But, a strong CPO could also result from deformation induced preferred alignment of elongated grains, both syn-/post-growth.

2. Objectives

- How do '*in-situ*' crystallized phases derived from the partial melt deform?
- Does rotation of '*in-situ*' crystallized phases impact their CPOs?
- Can '*oriented grain growth*', if any, influence intragranular deformation?

3. Deformation experiment

- Starting material - dry homogeneous mixture of Qz + Ms powder.
- Uniaxially cold pressed at 200 MPa, isostatically hot pressed at 160 MPa & 580 °C for 24 hrs. Torsionally deformed to finite shear (γ) 15.
- Confining pressure = 300 MPa; Temperature = 750 °C.
- Constant shear strain rate = 3×10^{-4} s^{-1}

Fig. 1. *Schematic illustration of a deformed cylindrical sample under torsion, cut along the longitudinal axial section. The black striped zones show the locations along which EBSD data were obtained.*

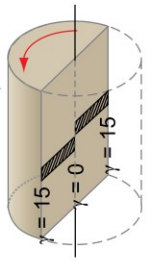

Fig. 2. *Block diagram representing one of the stripped zones showing the kinematic reference axes (XYZ), shear sense and the SEM image of the observed longitudinal axial section (YZ).*

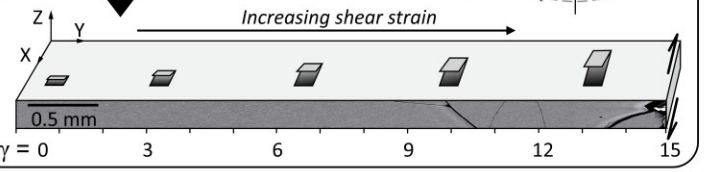

Mineral abbreviations: *Qz - Quartz; Ms - Muscovite; Kfs - K-Feldspar; Bt - Biotite; Ilm - Ilmenite; Mul - Mullite; Crd - Cordierite*

Pole figure reference frame

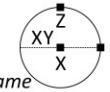

4. Electron backscatter diffraction

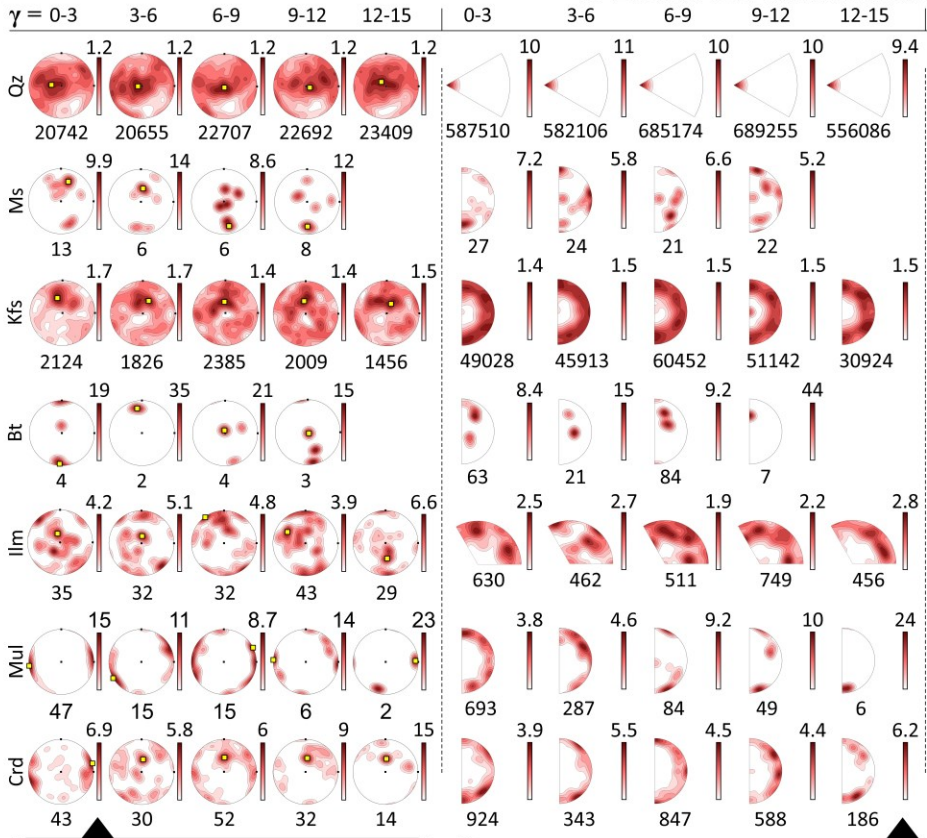

Fig. 3. *[001] pole figures at different γ. The stereoplots are lower hemispheric projections contoured to multiples of uniform density. Yellow squares indicate points of maximum densities. The values at the bottom of each pole figure refer to the total no. of grains.*

Fig. 4. *Distributions of the neighbor-pair high angle (> 10°) misorientation axes of the phases at different γ, on crystal coordinate systems. The values at the bottom of each plot refer to the no. of axes. Maximum densities are given by values on top of the scale bars. Bt & Ms grains are absent at subregions corresponding to highest γ.*

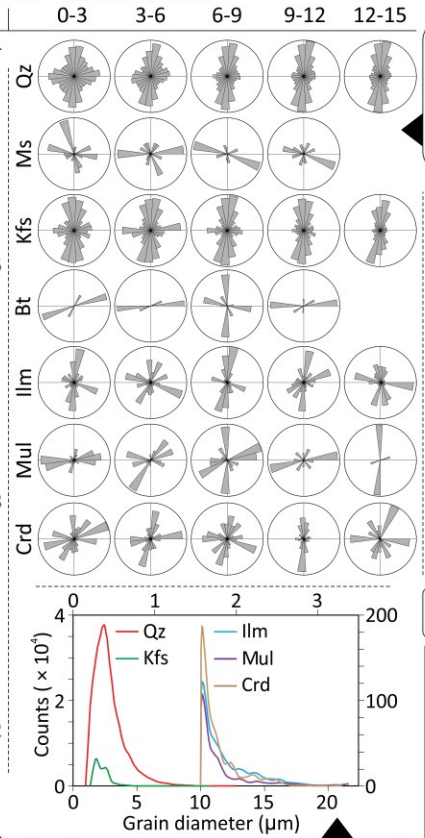

Fig. 5. *Rose diagrams showing the shape preferred orientations (long axis) of the grains of each phase **at different** γ. The horizontal and vertical lines in each of the rose plot represent the traces of the XY & XZ planes, respectively.*

Fig. 6. *Frequency distribution curves of grain diameters (area-equivalent). The left ordinate & bottom abscissa belong to the distribution of Qz & Kfs, whereas those of Ilm, Mul & Crd are represented by the right ordinate & top abscissa.*

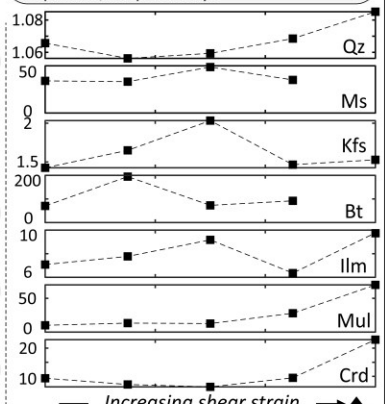

Fig. 7. *Variations in J-indices (J_{ODF}) for the different phases with increasing γ.*

5. Summary

- Equidimensional grains of melt-crystallized Kfs, Ilm, & Crd rotated during torsion. This was augmented by the surrounding melt.
- The rotation inhibited intracrystalline plasticity, producing relatively weak CPOs. It declined at γ > 7 as the crystal:melt ratio increased.
- '*Oriented growth*' along with shearing preferentially aligned the long axes of Bt, Ms & Mul grains parallel to the shear plane, resulting in their strong CPO.